New examples of Ru(ii)-tetrazolato complexes as thiocyanate-free sensitizers for dye-sensitized solar cells

New examples of Ru(II)-tetrazolato complexes as thiocyanate-free sensitizers for dye-sensitized solar cells

Valentina Fiorini, Edoardo Marchini, Mattia Averardi, Loris Giorgini, Sara Muzzioli, Angela Dellai, Roberto Argazzi, Alessandra Sanson, Nicola Sangiorgi, Stefano Caramori and Stefano Stagni

Dalton Transactions, 2020, 49, 15543-15555

The final published version is available online at: **https://doi.org/10.1039/c9dt02198a.**

Dalton Transactions

An international journal of inorganic chemistry

Accepted Manuscript

This article can be cited before page numbers have been issued, to do this please use: V. Fiorini, E. Marchini, M. Averardi, L. Giorgini, S. Muzzioli, A. Dellai, R. Argazzi, A. Sanson, N. Sangiorgi, S. Caramori and S. Stagni, *Dalton Trans.*, 2020, DOI: 10.1039/D0DT02621B.

ROYAL SOCIETY OF CHEMISTRY

rsc.li/dalton

New examples of Ru(II)-tetrazolato complexes as thiocyanate-free sensitizers for Dye-Sensitized Solar Cells

Valentina Fiorini,[a] Edoardo Marchini,[b] Mattia Averardi,[a] Loris Giorgini,[a] Sara Muzzioli,[a] Angela Dellai,[b] Roberto Argazzi,[b] Alessandra Sanson,[c] Nicola Sangiorgi,[c]* Stefano Caramori,[b]* Stefano Stagni [a]*

[a]: *Department of Industrial Chemistry "Toso Montanari", University of Bologna, Viale Risorgimento 4, I-40136 Bologna, Italy*
[b]: *Department of Chemical and Pharmaceutical Sciences, University of Ferrara, via Luigi Borsari 46, I-44121 Ferrara, Italy*
[c]: *Institute of Science and Technology for Ceramics, National Council of Research , ISTEC-CNR, Via Granarolo 64, I-48018 Faenza, Italy*

e-mail: nicola.sangiorgi@istec.cnr.it (Nicola Sangiorgi); cte@unife.it (Stefano Caramori); stefano.stagni@unibo.it (Stefano Stagni).

Abstract

A set of three new Ru(II) polypyridyl complexes decorated with 5-aryl tetrazolato ligands $(R\text{-}CN_4)^-$, (**D** series, namely **D1**, **D3** and **D4**), is presented herein. Whereas complex **D1** represents the pyrazinyl tetrazolato analogue of a previously reported Ru(II) complex (**D2**) with general formula cis-$[(dcbpy)_2Ru(N^N)]^+$, in which dcbpy is 2,2'-bipyridine-4,4'-dicarboxylic acid, and N^N is the chelating 2-pyridyl tetrazolato anion, the design of the unprecedented Ru(II) species **D3** and **D4** relied upon a completely different architecture. More specifically, the molecular structure of thiocyanate-based species cis-$[(dcbpy)_2Ru(NCS)_2]$, that is typically found in benchmark Ru(II) dyes for Dye Sensitized Solar Cells (DSSCs), was modified with the replacement of the two of the -NCS ligands in favour of the introduction of 5-aryl tetrazolato anions, such as the deprotonated form of 5-(4-bromophenyl)-1*H*-tetrazole, for complex **D3**, and 5-(4-cyanophenyl)-1*H*-tetrazole, in the case of complex **D4**. To streamline the behavior of the **D** series of Ru(II) complexes as photosensitizers for DSSCs, an in-depth analysis of the excited state properties of **D1**, **D3** and **D4** has been performed through TDDFT calculations and TDAS (nanosecond transient difference absorption spectroscopy). The obtained results highlight a trend that was confirmed once **D1**, **D3** and **D4** were tested as photosensitizers for DSSC under different conditions. Along the series of the Ru(II) complexes, the neutrally charged species **D3** and **D4** displayed the best photovoltaic performances.

DOI: 10.1039/D0DT02621B

Introduction

Over the past decade, intense research efforts have been devoted to the study of the coordination chemistry of tetrazole and tetrazolato based compounds, which have found application as building blocks for Metal Organic Frameworks (MOFs),[1] as well as nitrogen rich molecules for energetic materials,[2] and polytopic ligands for the construction of luminescent metal- and lanthanide based complexes.[3] In very recent times, the applicative scenario of these synthetically versatile nitrogen rich heterocycles has been extended to the third generation of photovoltaic technologies with the incorporation of tetrazolato based chelates, such as the 2-pyridyl tetrazolato anion,[4] within the structure of Ru(II) photosensitizers for Dye Sensitized Solar Cells application (DSSCs). Aiming at extending our past studies dealing with the preparation of photo and electrochemiluminescent Ru(II)-tetrazolato complexes to the design of new examples of tetrazolato-based DSSCs dyes, we now report the preparation and the characterization of new examples of Ru(II)-tetrazolato complexes, which differ both in the nature and in the coordinating mode adopted by the tetrazolato ligands (Figure 1). At first, we have slightly modified the structure of the Ru(II) tetrazolato-based dye reported by Dragonetti *et al.,*[4a] (complex **D2**, Figure 1), by replacing the 2-pyridyltetrazolato ligand with the 2-pyrazinyl tetrazolato anion (complex **D1**, Figure 1). Then, aiming at introducing an unprecedented class of tetrazolato-based Ru(II) dyes, the "traditional" molecular structure of thiocyanate-based Ru(II) dyes, cis-[$(dcbpy)_2Ru(NCS)_2$] – where dcbpy is 2,2'-bipyridine-4,4'-dicarboxylic acid - was modified with the replacement of the two of the -NCS ligands in favour of two 5-aryl tetrazolato anions, such as the deprotonated form of 5-(4-bromophenyl)-1*H*-tetrazole, for complex **D3**, and 5-(4-cyanophenyl)-1*H*-tetrazole, in the case of complex **D4**. (Figure 1) Further insights about the excited state nature and the charge transfer dynamics of **D1**, **D3** and **D4** on TiO_2 were obtained by combining TDDFT calculations with TDAS (transient difference absorption spectroscopy) in the ns-ms regime and DC/AC photoelectrochemical measurements with two different I^-/I_3^- based electrolytes.

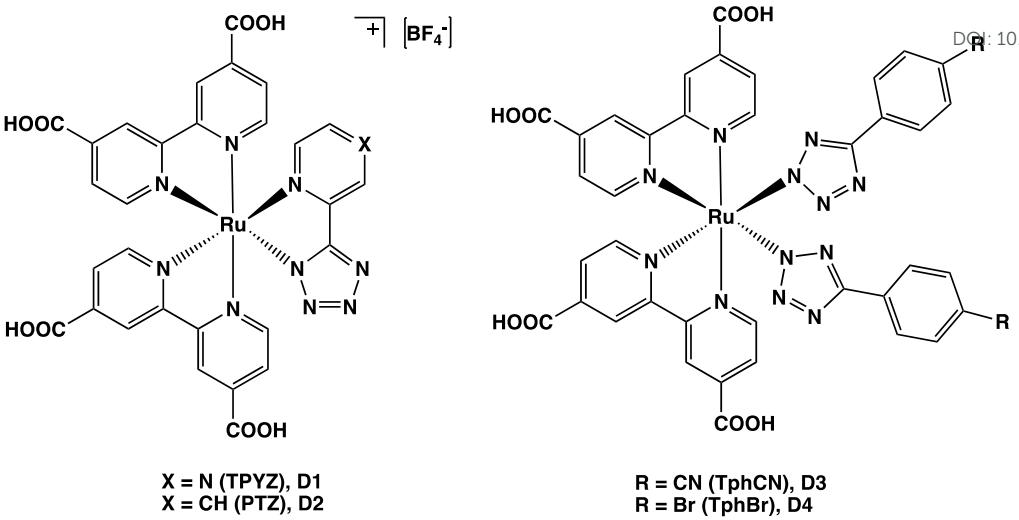

Figure 1*:* Ru(II) complexes described in this work and corresponding acronyms.

View Article Online
DOI: 10.1039/D0DT02621B

Results and Discussion

Synthesis, ESI-MS and NMR spectroscopy

The tetrazole ligands reported in this work have been prepared by following two slightly different methods, both of them involving the 1,3 dipolar cyclization of the azide anion (N_3^-) onto the appropriate nitrile precursor. More specifically, 2(1,H tetrazol-5yl) pyridine (H-**PTZ**), 2(1,H tetrazol-5-yl) pyrazine (H-**PYTZ**) and 5-(4-cyanophenyl)-1*H*-tetrazole (H-**TphCN**) were obtained in almost quantitative yield by adopting the procedure reported by Finnegan and co-workers,[5] while the preparation of of 5-(4-bromophenyl)-1*H*-tetrazole, (H-**TphBr**), was achieved through the method described by Koguro and co-workers.[6]

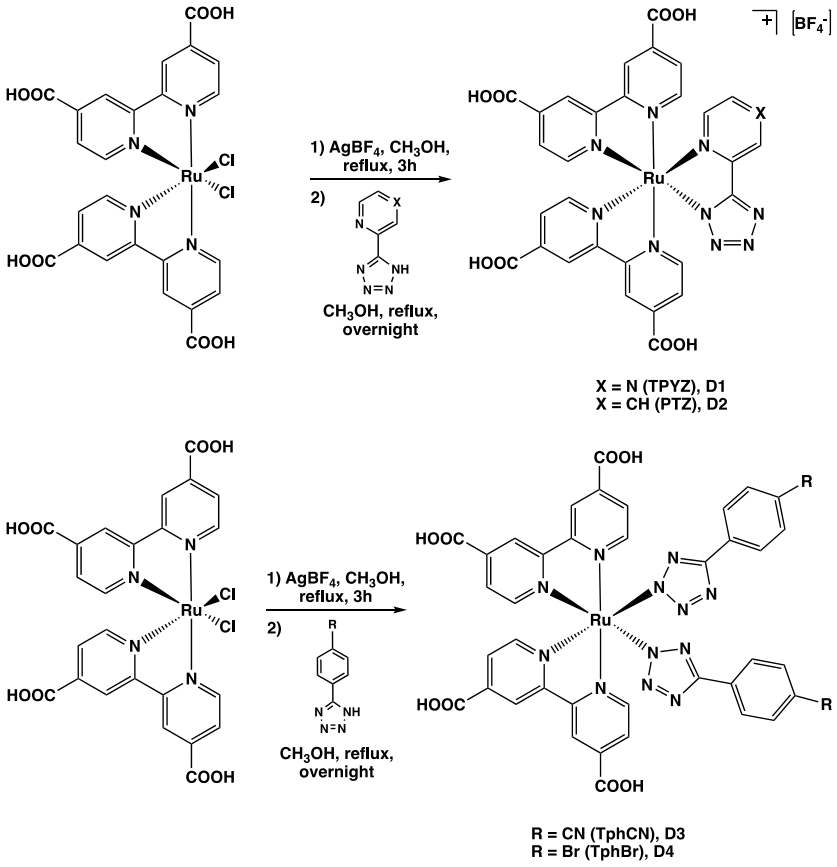

Scheme 1*:* Synthetic procedures for complexes **D1**-**4**.

The preparation of the Ru(II) species **D1-4** was accomplished by following a multistep procedure that involved at first halide extraction from *cis*-[Ru(dcbpy)$_2$Cl$_2$] (dcbpy = 2,2'-bipyridine-4,4'-dicarboxylic acid) with a molar excess of $AgBF_4$ in refluxing methanol. The removal of AgCl afforded a red filtrate that was then combined with the desired tetrazolate anion. After being heated at the reflux temperature overnight, the resulting mixtures were cooled to room temperature. The addition of a copious amount of diethyl ether to the reaction vessels caused the precipitation of the desired Ru(II) complexes, which did not require any further purification step. The identity of all the

View Article Online
DOI: 10.1039/D0DT02621B

Ru(II) complexes was at first deduced by ESI-Mass spectrometry, then confirmed by ^{1}H-NMR experiments, whose results confirmed the isolation of the desired products **D1-4**, since the corresponding ^{1}H-NMR spectra (Figure S1-S4 ESI) displayed a number of resonances congruent with their expected symmetry point group, i.e. C_s for **D1** and **D2**, C_2 for **D3** and **D4**.

Redox Properties

The redox properties of all the reported Ru(II)-based dyes **D1-4** has been investigated by performing cyclic voltammetry (CV) experiments on the corresponding CH_3OH/CH_3CN 1:1 solutions (Table 1).

Table 1: Half-Wave Redox Potentials[a] ($E_{1/2}$) of all the Ru(II) species presented in this work at 25 °C, CH_3OH/CH_3CN 1:1.

Complex	E / V		E_{HOMO}[c]	E_{LUMO}[c]
	oxidation[a,b]	reduction[a,b]	(eV)	(eV)
D1	+1.31 (0.98)	-1.01 (-1.34)	-5.91	-3.59
D2	+1.02 (0.69)	-1.01 (-1.34)	-5.62	-3.59
D3	+1.30 (0.97)	-1.36 (-1.69)	-5.90	-3.24
D4	+1.07 (0.74)	-1.59 (-1.93)	-5.67	-3.01
N719	+1.07 (0.74)	-1.46 (-1.79)		

[a] In a 0.1 M $TBAPF_6$/ CH_3OH/CH_3CN 1:1 solution, [b] $E_{1/2}$ vs SCE, (vs. Fc+/Fc); $E_{1/2}$ (Fc^+/Fc) = 0.33 V vs SCE. [c] calculated with $E_{HOMO} = -(e*E_{ox} + 4.6\ [eV])$ and $E_{LUMO} = -(e*E_{red} + 4.6\ [eV])$,[7] where e is the unitary charge [1C].

All the reported species exhibited a single oxidation in the region of positive potentials, which was assigned to the Ru(II)/Ru(III) process (see ESI figures S14-17). In good agreement with the data that were reported previously for similar Ru(II) polypyridyl complexes such as $[(bpy)_2Ru(PTZ)]^+$ and $[(bpy)_2Ru(TPYZ)]^+$,[8] where bpy is 2,2' bipyridine, the oxidation (vs SCE) of **D1** occurs at more positive potentials (+1.31 V) than that of **D2** (+1.02 V), according to the remarkable electron withdrawing character of the pyrazine ring (**TPYZ**) with respect to the pyridyl tetrazolato (**PTZ**) moiety used in the design of **D2**. A similar trend emerged from the CV curves of the neutral dyes **D3** and **D4**. Given the pronounced electron withdrawing character of the cyanide group of **TphCN**, if compared to that of the bromine substituent of **TphBr** (complex **D4**), the oxidation peak of **D3** was found at more positive potentials (+1.30 V) with respect to **D4** (+1.07 V). With regards to negative potentials, the CV investigation has been carried out by exploring the first visible reduction (see ESI figures S14-17). In the case of the positively charged Ru(II), the first process occurs at the same potential (-1.01 V) for both **D1** and **D2**. In the case of the neutral dyes **D3** and **D4**, a displacement of the first reductive processes to more negative potentials was observed (-1.36 V for **D3** and -1.56 V for **D4**), in good agreement with the electronic effects that are brought by the bromine substituent). As a

comparison, the Ru(II)/(III) process for N719 falls at *ca.* +1.07 V, while the dcbpy -based reduction was found at *ca.* -1.46 V vs SCE in our experimental conditions. This ca. 200 mV anodic shift of the Ru(II)/Ru(III) compared to literature values in pure ACN, [9] could be explained by the lower Lewis basicity of the MeOH/ACN, which makes the NCS ligands stronger electron acceptors via second sphere interactions.

Electronic Spectroscopy

The absorption spectra of **D1-4** were obtained at room temperature from the corresponding methanol CH_3OH (10^{-4}M) solutions, and are depicted in Figure 2. For all the Ru(II) species, the absorption profile typically displays intense bands in the UV region (200-350 nm) which are assigned to LC (*ligand centred*) dcbpy-based π-π^* transitions. Weaker absorption are found from 450 to 510 nm (visible region, Figure 2) and are ascribed to MLCT-type (*metal to ligand charge transfer*) transitions, involving the Ru(II) metal centre and both the dcbpy and the tetrazolato -based ligands. These assignments have been further circumstantiated with theoretical TDDFT calculations (see later on).

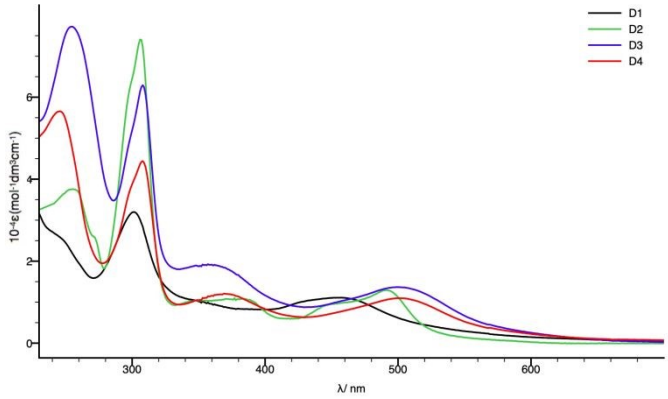

Sample CH_3OH	Abs λ_{max} (nm), $10^{-4}(\varepsilon)$
D1	302 (3.19), 454 (1.11)
D2	256 (3.57), 305 (7.40), 384 (1.07), 493 (1.28)
D3	254 (7.71), 308 (6.29), 362 (1.91), 500 (1.37)
D4	247 (5.64), 307 (4.42), 370 (1.20), 501 (1.09)

Figure 2*:* Absorption spectra and relevant data of Ru(II) tetrazolato dyes, 10^{-4}M, CH_3OH.

The UV-vis absorption feature of the Ru(II) complexes **D1-4** were compared those of the standard dye N719, [10] which exhibits in our experimental conditions an absorption profile with λ_{max} = 525 nm ($\varepsilon = 1.26 \times 10^4\ M^{-1}\ cm^{-1}$). At first glance, the comparison between N719 and **D1-D4** results in the *hypsochromic* shift of the MLCT band (Table 1) for all the complexes, enlightening a more pronounced variation for **D1** ($\Delta\lambda$ = *ca.* 70 nm), while a less evident *albeit* significant shift to lower wavelength ($\Delta\lambda$ = 20-30 nm) of the ^{1}MLCT maxima was detected for **D2**, **D3** and **D4**. In this regard, the differences in MLCT-based absorption maximum between **D1** and **D2** can be attributed to the more electron withdrawing character of the pyrazine ring of **D1**. No substantial differences were

found from the comparison of the spectra of benzonitrile and bromobenzene appended complexes - **D3** and **D4**, which both displayed an absorption maximum centred at *ca.* 500 nm. All the Ru(II) species of the series **D1**-**D4** are spontaneously adsorbed on TiO_2 films during a traditional sensitization process, giving rise to sensitized photoanodes capable to absorb up to *ca.* 90% of incident photons around 500 nm in the case of **D3** and **D4** (Figure 3). The light harvesting ability of **D1** is much less satisfactory, owing to its smaller absorptivity (ε) and lower solubility in the chosen solvent medium which may limit the dye uptake. All the **D**-type complexes retain their spectral characteristics once loaded on the solid thin films, displaying the same spectral shape and nearly unaffected absorption maxima as in solution. Thus, the outcome of the spectroscopic and electrochemical experiments that were performed in fluid solution might be confidently extended to the sensitizer moieties bound to the semiconductor surface. Finally, the absorption profiles obtained from the series of Ru(II) species **D1-D4** are substantially blue shifted with respect to the one of the reference compound N719, whose lowest energy MLCT band is centred at *ca.* 550 nm and tails off beyond 700 nm, *i.e.* the low energy region in which the harvesting from the species **D3** and **D4** becomes negligible.

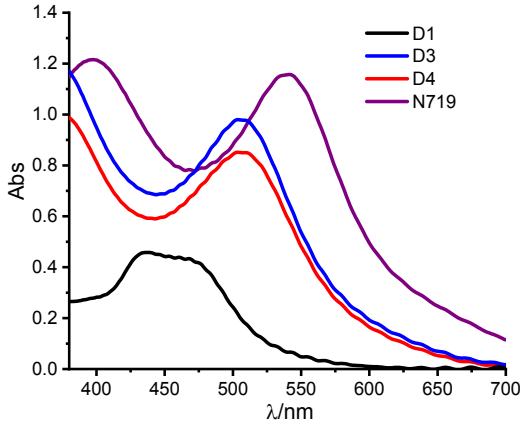

Figure 3. Absorption spectra of the complexes D1-D4 loaded on transparent TiO_2 films (ca. 6 µm thick) sintered on FTO. Spectra were corrected against a background constituted by an otherwise identical undyed TiO_2/FTO film.

TDDFT calculations

TDDFT calculations were run on the optimized structures of complexes **D1**, **D3**, **D4** and N719 for comparison. The frontier orbitals involved in the main visible transitions are reported in Figure S1, ESI. We selected the PBE0 functional for being reported as benchmark [11] to reproduce accurately the equilibrium geometries of many Ru(II) complexes. The DGDZVP basis set was proved valuable for studying the optical and electronic properties of Ru polypyridine compounds,[12] while the bulk

View Article Online
DOI: 10.1039/D0DT02621B

solvation properties were described in the framework of the continuum polarization model.[13] The calculation qualitatively reproduces the experimental trend in HOMO energy obtained from cyclic voltammetry, following the series **D1**>**D3**>**D4**. Also, the **D** series exhibits a deeper HOMO energy than N719, in agreement with both experimental data and with the expected stronger electron withdrawing effect exerted by the tetrazolato ligands. The calculation predicts the LUMOs energy to be quite similar in **D3**, **D4** and **N719**, being mainly localized on the same dcbpy moieties, while the first **D1**'s empty orbitals are *ca.* 300 meV lower than the formers. These results are in good agreement with the relative experimental trend found in the reduction potentials (Table 1), although the comparison with the CV values should be taken with some caution, due to the irreversible electrochemical behavior originated by the first reduction processes localized on the dcbpy ligand.[14] A comparison between the lowest 25 vertical transitions and the experimental spectrum are reported in Figure 4.

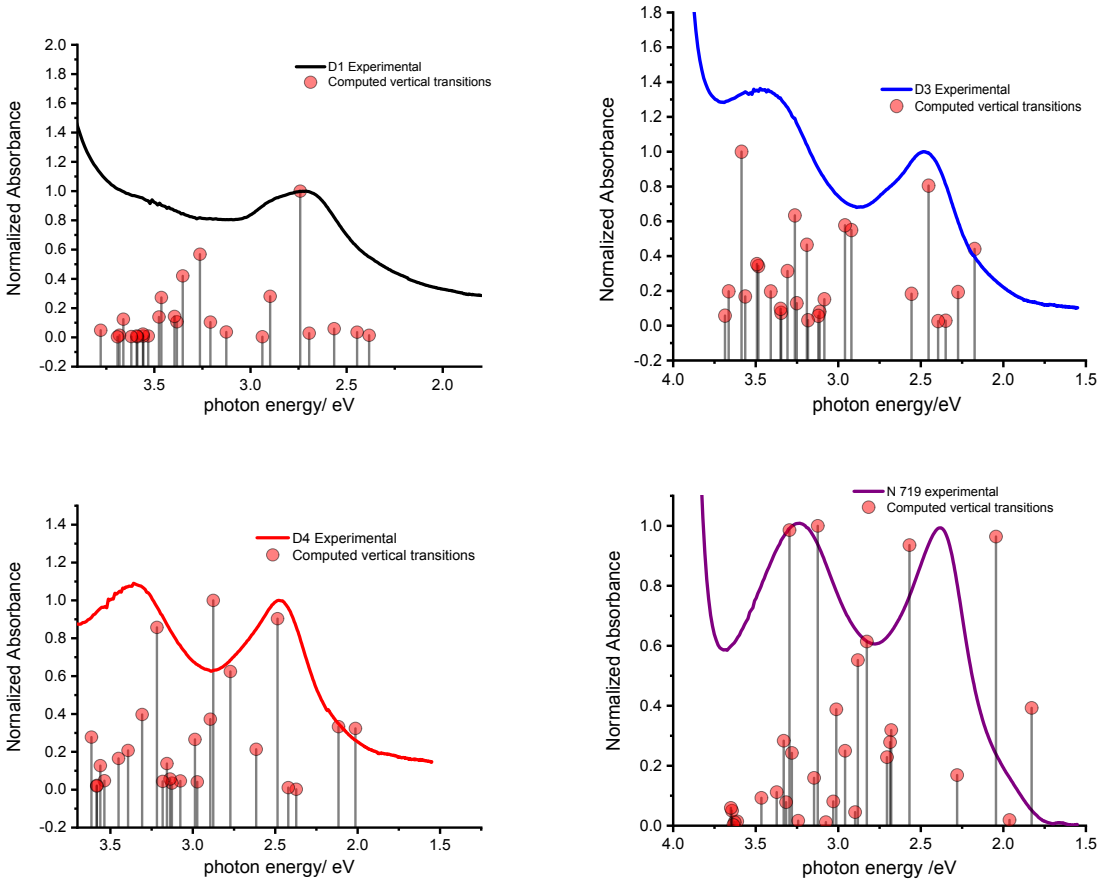

Figure 4. Experimental (black, blue, red and purple) vs TDDFT/PBE0/DGDZVP computed optical transitions (vertical grey lines surmounted by red circles) in the complexes D1-D4 (from left to right) compared to N719 (bottom right). Experimental spectra were normalized to the lowest absorption band, while vertical transitions were normalized to the most intense one.

View Article Online
DOI: 10.1039/D0DT02621B

The TDDFT/PBE0/DGDZVP calculations reproduces the experimental optical absorption of all the complexes quite accurately, showing transitions clustered around 2.5 and 3.3 eV, coincident with the experimental main absorption band of all compounds. The most intense computed vertical transitions overlap well with the respective maximum of the lowest energy experimental absorption band, found at 2.74 eV in the case of **D1** and at *ca.* 2.5 eV for **D3** and **D4**. Clearly, the low energy tail of the experimental absorption spectra, which bears also spin forbidden excitations to triplet states, is less satisfactorily described by this type of TDDFT calculation, which only includes excitations with the same spin multiplicity as that of the singlet ground state (S_0). The matching with the experimental spectrum of N719 is also reasonably good, as groups of transitions centered around 3.25 and 2.2 eV are observed. In the case of N719 the computed transitions appear to be correctly red shifted with respect to those of **D1**, **D3** and **D4**, showing the lowest transitions at *ca.* 1.8 eV, in good agreement with the experimental absorption onset of such compound. The main contributions to the optical transitions involve mixed excitations from the frontier orbitals HOMO, HOMO-1 and HOMO-2 orbitals to LUMO, LUMO +1 and LUMO +2, whose energy levels and isodensity maps are depicted in Figure S5 and S6, ESI. In the case of **D4** excitations from HOMO-3 to LUMO +3 are also contributing to visible absorption. In all cases, the lowest virtual orbitals are mainly localized on the dcbpy ligands whose energy is thus nearly the same for the whole series under investigations. The relevant occupied orbitals bear contributions from atomic orbitals of the Ru(II) metal centre, which may mix with both σ and π system of the ancillary ligands. In the case of N719, the expected strong mixing with the π system of the NCS groups is observed,[15] and indeed the sulfur atoms of the NCS contribute the most (up to 45 %) to the amplitude of the highest occupied orbital. In the case of **D1** and **D4**, orbital mixing with the ancillary ligands is much less substantial. Thus, while in the case of N719 visible absorption bears the contribution from mixed MLCT and LLCT (Ligand to Ligand Charge Transfer) states, in the case of **D1**-**D4** series we observe more classical MLCT states where the electron is mainly excited from metal centered orbitals to empty orbitals having π character localized on the dcbpy ligands. This is confirmed by EDDM (Electron Density Difference Maps) of the lowest visible excitation (Figure 5), which corresponds to the charge distribution in terms of electron and hole density in the lowest excited state (*i.e*. the S_1 state) of each dye, from which charge injection is likely to occur.

View Article Online
DOI: 10.1039/D0DT02621B

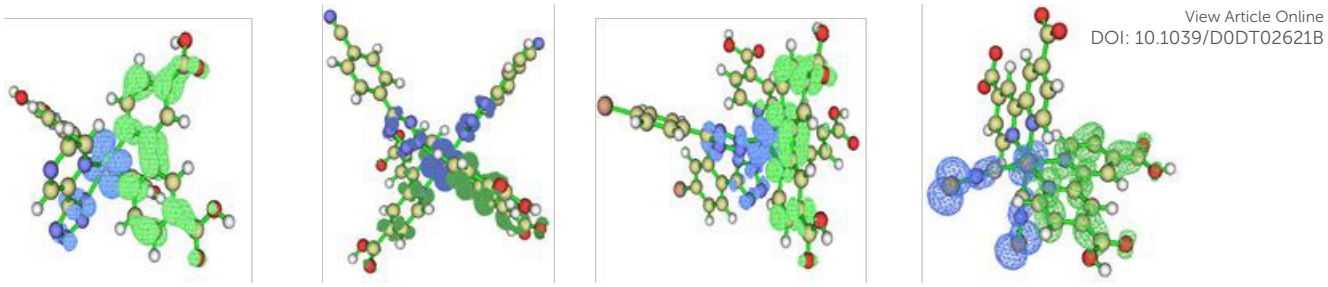

Figure 5. EDDMs resulting from the lowest energy optical excitation of complexes D1, D3 and D4 compared to N719 (left to right). The green surfaces depict increased electron density (*i.e.* electron localization) while blue surfaces indicate regions of depleted electron density (*i.e.* hole localization).

EDDMs clearly reveals that in all cases, in the lowest excited state (S_1) the electron is localized onto the dcbpy moiety, which shows a substantial involvement of the -COOH anchoring group allowing a favorable coupling for electron transfer to TiO_2. (Figure 5). On the other hand, hole density is principally localized on the Ru(II) core for **D1**, **D3** and **D4**, where, however **D3** and **D4** present also a significant mixing with orbitals of the 5-aryl-tetrazolato moieties. The shorter transition dipole moment of **D1**, compared to **D3** and **D4** may explain the relatively low extinction coefficient of the former. When a given dye is attached to TiO_2, hole delocalization on the ancillary ligands which are directed far from the surface (see for example the molecular mechanics models in Figure S7 ESI), favours long lived charge separation, by spatially decoupling the hole centred on the molecular moiety from the photoinjected electron in the density of acceptor states of TiO_2. Unrestricted PBE0/DGDZVP calculations on the oxidized molecular species (formally Ru(III) species) introduce the effect of orbital relaxation due to the formation of a positive charge on the molecular dyes following electron injection. These calculations indicate that the involvement of the tetrazolato ancillary ligand is more substantial than what can be anticipated from the analysis of EDDMs, representing the charge distribution in the lowest singlet excited state. The involvement of the non-chromophoric ligands in the HSOMO (Highest Singly Occupied Molecular Orbital, Figure 6), which essentially describes the spatial hole distribution, varies in the order N719 (NCS) > **D4** (TPhBr) > **D3** (TphCN) > **D1** (TPYZ). In Table S1 are reported the single atom contribution to the HSOMOs of each dye, showing that the amplitude of such wavefunction on the Ru atoms decreases in the order **D1** > **D3** > **D4** > **N719**, in agreement with the increasing extent of delocalization on the ancillary ligand. Besides retarding back recombination, hole delocalization on the ancillary ligands can be crucial in accelerating the regeneration kinetics by the electrolyte, by exposing most of the hole density to diffusing iodide ions acting as electron donors in solution.

View Article Online
DOI: 10.1039/D0DT02621B

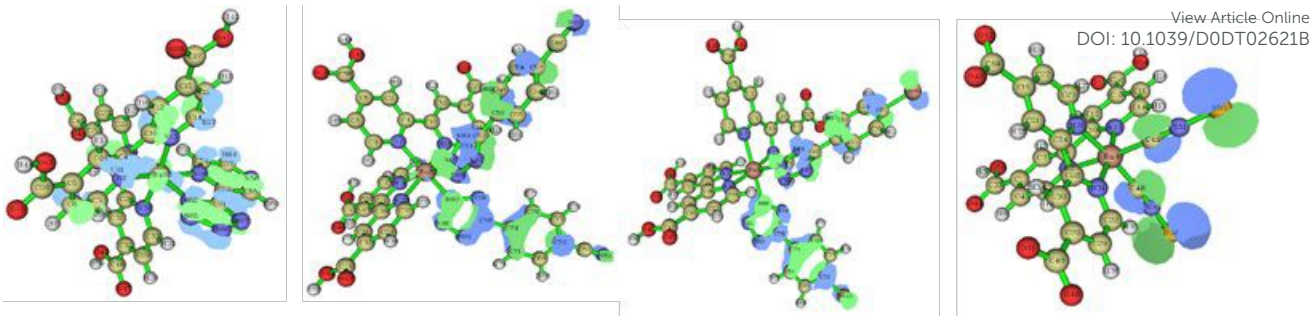

Figure 6. HSOMO isodensity surfaces for the **D1**, **D3** and **D4** dyes in the oxidized form compared with N719 (left to right respectively).

Time Resolved Spectroscopy

Nanosecond transient difference absorption spectra (TDAS) of the complexes **D1**, **D3** and **D4** in solution are reported in Figure S9, ESI. With the sole exception of **D1**, whose poor solubility demanded the addition of few drops of TBAOH, all spectra were measured in CH_3OH. To avoid possible sample degradation upon UV exposure, a 400 nm cut off filter was placed in front of the probe beam, thus the spectral analysis was restricted to the 400-800 nm range. Each dye displayed a mono exponential excited state decay kinetic, with lifetimes, under aerated conditions, that varied according to the sequence **D4** (108 ns) > **D3** (60 ns) > **D1** (33 ns) > N719 (*ca.* 8 ns). The excited state features were typical for the formation of a triplet MLCT/LLCT state in Ru (II) compounds, which is populated in a sub-nanosecond time scale, showing a broad ground state bleaching which extends from 400 and 600 nm and mirrors almost exactly the main visible bands of the complexes, which peak at *ca.* 450 nm in the case of **D1**, 500 nm for **D3** and *ca.* 510 nm for **D4**. The transient spectrum of N719 is short lived and partially convolved within the instrumental response function. Nevertheless, the bleach of the MLCT/LLCT bands is clearly observed, followed by triplet state absorption between 650 and 750 nm and by a bleach caused by spontaneous emission rising up for $\lambda > 750$ nm. Triplet absorption is quite less evident for the **D** series compounds, being mostly offset by the stronger spontaneous emission (phosphorescence) causing a broad bleaching band to appear for $\lambda > 600$ nm, in agreement with the steady state emission spectra acquired at r.t. in solution (Figure S8 ESI). In general, the longer lifetime exhibited by the **D** series compared to N719 can be qualitatively explained on the basis of the energy gap law [16] and by the coordination sphere in N719, which bears two anionic NCS ligands, which, through the establishment of stronger second sphere solvation effects, facilitate vibrational funneling of the electronic energy and collisional relaxation. Electron injection is known to be very efficient for many Ru(II) compounds, like the benchmark compound N719, providing a sufficiently negative excited state oxidation potential

View Article Online
DOI: 10.1039/D0DT02621B

(E^*_{ox}) and a proper excited state directionality. Injection from the lowest singlet state S_1 is confined within a fs time scale, while injection from the lowest triplet state T_1 is still fast compared to other deactivation pathways, being reported in the 1-100 ps time frame.[17] Injection from the T_1 state is actually believed to be the dominant one in a real DSSC, owing to the dynamics caused by the interlacing of several interacting chemical components (semiconductor, Dye, electrolyte having a complex formulation).[18] In our case, E^*_{ox} values of the **D** series are quite comparable with that reported for N719. Singlet excited state redox potentials ($^SE_{ox}$*) range between -1.07 V vs SCE (**D1**) and -0.87 V vs SCE (**D3**), while triplet potentials $^TE_{ox}$* are in the order of 200-300 mV lower. Figure 7 summarizes the thermodynamic levels relevant to the DSSC functioning, expressed on the electrochemical potential scale vs SCE, pictured at open circuit along with the N719 levels, in good agreement with literature data [10], [18], taken in the same experimental conditions as those of the **D** series. The flat band potential (E_F) of TiO_2 is represented at ca. -0.7 V vs SCE, a commonly accepted value in the organic DSSC electrolytes [19] along with the density of states (DOS) of TiO_2, $\left(DOS \propto e^{\frac{E}{E0}}\right)$. [20] E_0 is an experimental potential parameter ranging between 50 and 100 mV and E should be taken in absolute value. The TiO_2 DOS stretches across the semiconductor conduction band edge and its occupancy is related to the quasi-Fermi energy of the semiconductor. Generally speaking, the singlet excited state potentials of the **D**'s singlet states are quite aligned with that of N719, and also the triplet states, with the exception of **D3,** are comparable or slightly better reductants. As a consequence, with the good excited state directionality observed before, we expect a satisfactory coupling with the acceptor states of the TiO_2 and efficient injection under short circuit (sc) condition (TiO_2 Fermi level equilibrated with E_{redox}). We note that the injection kinetics is relatively independent by the increase in photovoltage (forward bias) unless the density of states does not shift as a whole, due to the presence of TiO_2 potential determining ions or other additives (band edge modifiers) in the electrolyte composition.

View Article Online
DOI: 10.1039/D0DT02621B

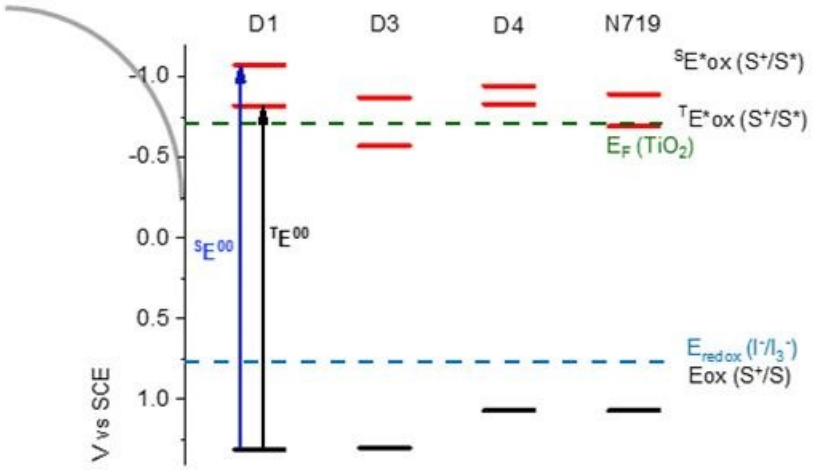

Figure 7. Ground and excited state oxidation potentials of the dyes under consideration (Data from table 1 and Figure S4) compared to the TiO_2 flat band potential in an organic solvent and to the equilibrium potential of a typical iodide based electrolyte.

This is due to the fact that the DOS increases exponentially with energy, and despite its partial filling due to electron injection, there is always a sufficient number of available acceptor states in the semiconductor to ensure efficient quenching of the excited states by electron transfer. Clearly, the overlap of the DOS with the T_1 states is lower and, in general, injection from the triplet state will be slower. This drawback is however well balanced by the much longer T_1 lifetime with respect to S_1. Concerning dye regeneration by the iodide based redox couple, ($S^+ + 2\ I^- \rightarrow S + I_2^{\cdot-}$, for example), the **D** family displays a stronger driving force than N719, which should guarantee efficient regeneration despite the less favorable HSOMO localization in the **D** series with respect to N719.[21]

TDA spectroscopy on thin films in contact with 0.1 M Li^+ in CH_3CN (Figure 8), revealed the absence of spontaneous emission and, as main spectral features, the complete bleaching of the ground state absorption owing to MLCT/LLCT transitions and the contemporary appearance of a broad absorption rising for λ > 600 nm, which is more evident in the **D3**, **D4** and **N719** species while less pronounced for **D1**. These transient spectra evolve in time, following a multiexponential (at least bi exponential) kinetics without changes in their relative spectral shape, up to the ms time scale. All these properties are consistent with the formation of the long lived charge separated state (Ru(III)-e^- (TiO_2)) whose decay by recombination is still incomplete within the 5 ms time window chosen for these experiments. Formation of this state is always within the instrumental response of the spectrometer even when operated at its maximum resolution (FWHM *ca*. 7 ns) while the absence

View Article Online
DOI: 10.1039/D0DT02621B

of any detectable residual of spontaneous emission indicates that electron transfer is the dominant excited state quenching pathway once these dyes are attached to TiO_2.

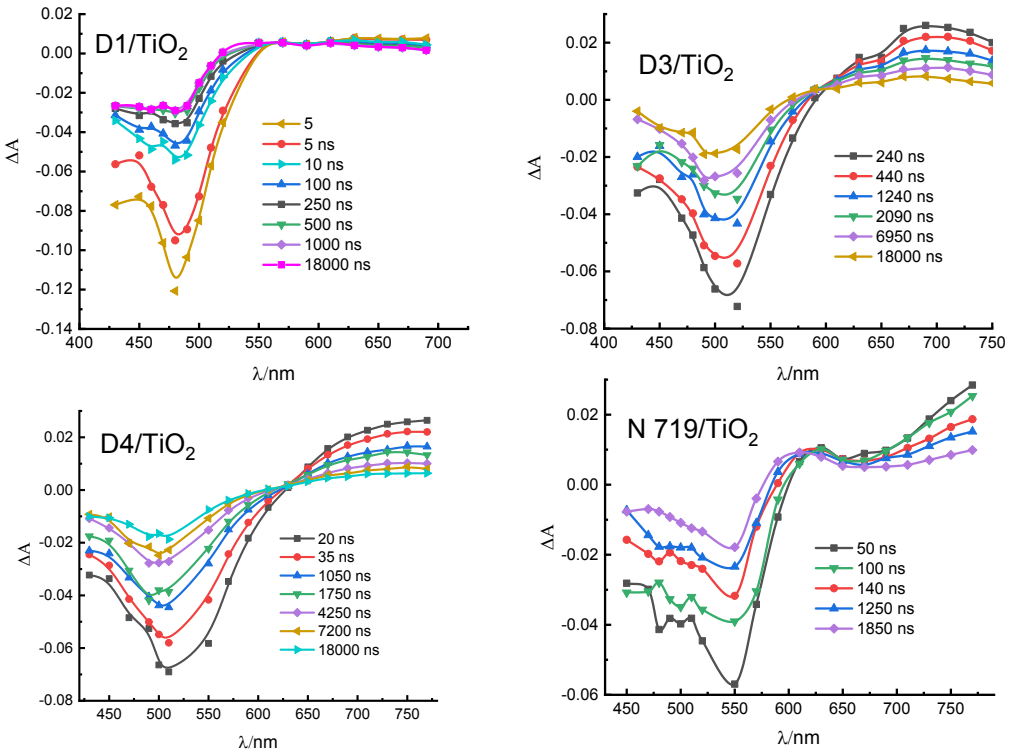

Figure 8. ns-µs transient absorption difference spectra of the D-dyes loaded on transparent TiO_2 thin films (Dyesol-18NRT) in contact with acetonitrile containing 0.1 M $LiClO_4$. N719 in ethanol is also reported as a comparison. Oscilloscope input impedance 350 Ohm. N719 is included as a comparison.

For the whole **D** series, Ru(II) regeneration by iodide (0.1M LiI, 0.6 M PMII and 0.05M MgI_2 in CH_3CN) is generally fast compared to recombination (Figure S10 ESI), being mostly complete within 10^{-5}-10^{-4} s time scale, while recombination is at least one order of magnitude longer, extending well into the ms time scale. This agrees with the strong oxidant power of the ground state of the **D** complexes, making electron donation exoergonic by at least 0.6 eV. Regeneration efficiency, η_{reg}, (η_{reg}= (k_{reg}/(k_{reg} + k_{rec}) where k_{reg} and k_{rec} are pseudo-first order rate constants extracted from the amplitude weighted time constants obtained from the biexponential fits,[22] stands at 98% for **D3** and **D4**, while sits around 80 % in the case of **D1**. Regeneration of N719 is also quantitative and mostly occurs within the instrumental time response of the spectrometer (FWHM *ca*. 1 µs, base 4 µs), when pre-amplified by the 10 kΩ input impedance. The faster Ru(II) regeneration kinetics observed in the case of **D3** and **D4** may arise from the better delocalization of holes on **TphBr** and **TphCN** tetrazolato ligands, which allows a better electronic coupling with I^-, an essential requirement in speeding up the electron donation.

View Article Online
DOI: 10.1039/D0DT02621B

Photoelectrochemistry

JV curves, IPCE and APCE spectra were collected with sandwich transparent DSSCs, equipped with PEDOT -coated counter electrodes and based on the CFE electrolyte (0.1M LiI, 0.6M PMII, 0.05M MgI_2 and 0.1 M I_2 in CH_3CN, Figure 9). CFE, an high performance electrolyte enriched with Li^+ and Mg^{2+}, is tailored to emphasize photocurrent at the expense of photovoltage, which is useful to probe the sensitization properties of the dyes in conditions similar to those used for transient spectroscopy. Both Li^+ and Mg^{2+} downshift the TiO_2 DOS favoring charge injection,[23] while the excess of I^- (0.7 M) with respect to I_2 (0.1 M), together with the low viscosity of the electrolyte, promote an efficient regeneration of Ru(III). Clearly, CFE is not suited for long term stability of the DSSC, owing to CH_3CN volatility and relatively low I_2 concentration, the latter being a species which is depleted from the electrolyte during prolonged cell operation, in particular when heated and/or polarized under reverse bias.[24]

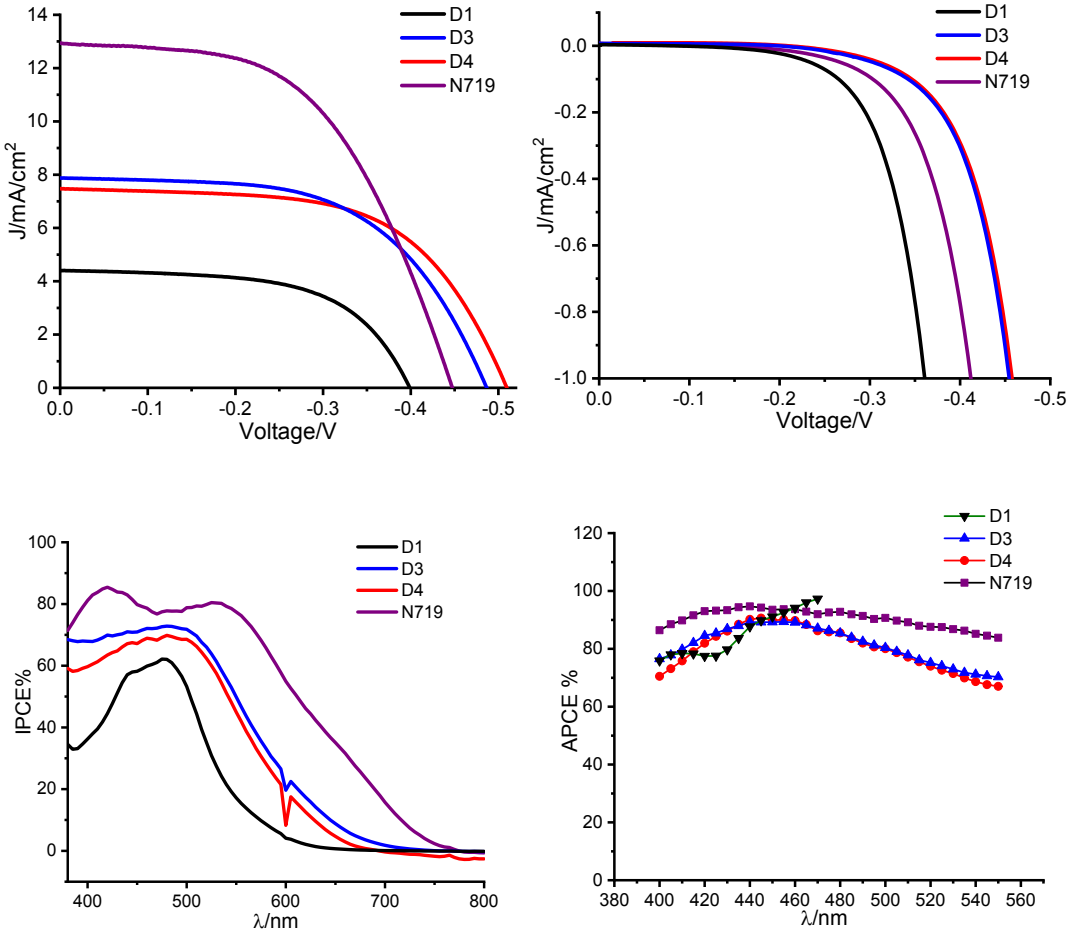

Figure 9. J-V curves collected under AM 1.5G illumination (top left), under dark conditions (top right), IPCE spectra under short circuit (bottom left) and APCE spectra (APCE=IPCE/LHE) (bottom right) computed from data (bottom left) and Figure 3. The APCE spectra were restricted to the spectral region enclosing the visible band maximum, where the error in the estimation of the LHE is the smallest.

The performance of the **D** dyes varies with the order **D4**>**D3**>**D1** (Figure 8a). **D3** produces the best photocurrent (≈ 8 mA/cm^2), but **D4** presents the best photovoltage value. Both **D3** and **D4** exceed N719 in photovoltage, consistent with dark currents varying in the order **D3**≈**D4** < N719 < **D1**. This trend could be explained by the greater shielding exerted by **TphBr** and **TphCN** pendants on the TiO_2 surface, which partially screen the semiconductor surface from the approach of the I_3^- electron acceptor. In the case of **D1** this is less effective, probably due to both lower steric hindrance of the **TPYZ** ligand with respect to the formers and to the lower surface loading caused by solubility issues. The lower photocurrent observed for the **D** sensitizers with respect to N719 appears to be mainly motivated by light harvesting. Indeed, as clearly shown by the photoaction spectra (IPCE vs λ, Figure 8c), N719 extends its photoconversion up to 770 nm, while for **D3** and **D4 it** is restricted at wavelengths < 700 nm and, when compared to N719, drops significantly in the 550-700 nm region, consistent with their absorption spectra (Figure 3). Normalization of the IPCE for the Light Harvesting Efficiency (LHE (λ) = $1\text{-}10^{-A(\lambda)}$, where A is the absorbance of the background corrected transparent sensitized film) affords the APCE or IQE figure (APCE = $\Phi_{inj} \times \eta_{reg}$ where Φ_{inj} is the injection quantum efficiency and η_{reg} is the regeneration efficiency measured under short circuit). APCE values ranging between 90% and 80% are in good agreement with the η_{reg} values estimated from transient spectroscopy and are consistent with good injection yields (80-90%) for **D1**-**D4**, expected on the basis of their excited state oxidation potentials.

APCE also corroborates the indication that the low performance of **D1** is mostly explained by its poor light harvesting and blue shifted response, together with its lowest η_{reg}. APCE also shows that the **D3** and **D4** response is slightly lower than that of N719; taking into account that η_{reg} ≈1, this could be indicative of a slightly lower injection efficiency from excited states, which are less sensitive to the solvent environment than N719, which bears NCS groups able to establish second sphere interactions with the solvent medium. Indeed, in contact with pure ACN (the solvent of the CFE formulation) the excited states of N 719 become significantly better reductants, owing to a cathodic shift of ca. 200 mV of the Ru(II)/(III) potential. This limitation of the **D** series could be exacerbated when using different electrolyte formulations containing a lower amount of TiO_2 potential determining cations like Li^+ and Mg^{2+}.

The analysis of the photoelectrochemical performance was thus extended to solar cells built with commercially available materials and filled with a high stability electrolyte with a formulation optimized for N719 (“Iodolyte Z-100”, Solaronix). Details of the electrolyte formulation are not disclosed by the producer, but in general it contains basic additives to enhance photovoltage, a

View Article Online
DOI: 10.1039/D0DT02621B

greater amount of I_2 and Ionic Liquids with a lower volatility as I^- source. The J-V curves of the Ru(II) dyes **D1** - **D4** and N719 obtained under AM 1.5G solar simulator, as well as the IPCE values, are reported in Figure S11-S13, together with the resulting efficiency figures in Table S1, ESI. With "Iodolyte Z-100" as electrolyte, a decrease in photocurrent density and IPCE value were observed for all dyes including N719. On the contrary, an increase in photovoltage and in Fill Factor was detected. A comparison between CFE and "Iodolyte Z-100" reveal that the decrease in photocurrent is quite modest for N719, but significant for the **D** series (by a factor at least ×2). The shift in photovoltage is motivated by the presence of basic additives which shift the flat band potential of TiO_2, while the lower photocurrent and higher iodine content are favorable to enhance the Fill Factor. The gain in photovoltage with respect to CFE is significant with N719 (ca. 250 mV), but much less evident for the **D** sensitizers, due to the strongly reduced photocurrent density which suggests a less effective injection and regeneration of Ru(III) in such electrolyte. TDA spectroscopy carried out in the presence of "Iodolyte Z-100" reveals the formation of Ru(III), but regeneration appears to be slower, being incomplete in the 0.1 ms timescale. Also in these conditions we can confirm that **D4** is the best sensitizer among the tetrazolato series, owing to the best combination of ground and excited state oxidation potentials and light harvesting, which was confirmed by Electrochemical Impedance Spectroscopy analyses (EIS, Figure 10).

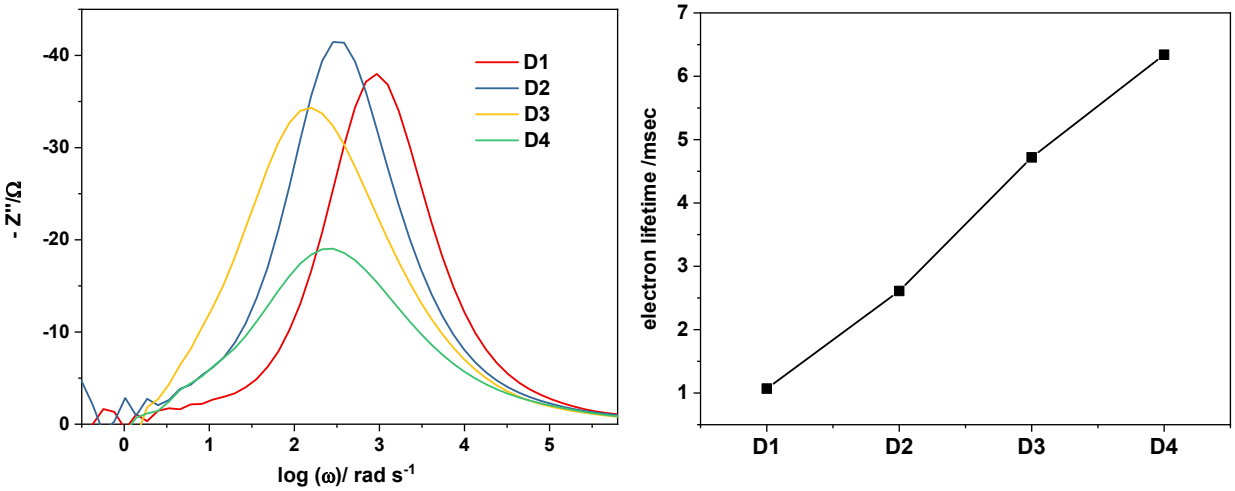

Figure 10. (left) Imaginary impedance plot of the EIS analyses and (right) calculated electron lifetime.

In the dark and in the presence of a forward voltage equal to the open circuit voltage (V_{OC}) recorded under illumination, EIS provides the negative of the imaginary part of Z (-Z'') vs. log(ω) plot from which one can obtain the TiO_2 electron lifetime (τ) defined by $\tau = \frac{1}{\omega_{max}}$ (Figure 10 left) [25], where

ω_{max} is the angular frequency at which the –Z'' peak is observed. This time constant depends on the charge recombination rate that occurs between TiO_2 sensitized films and the "Iodolyte Z-100" electrolyte. [26]

In agreement with the results obtained from the photoelectrochemical characterization, the calculated electron lifetime values values (Figure 10 right) suggest that dyes **D3** and **D4** are the most suitable Ru(II) complexes for DSSC fabrication in the **D** series described herein.

Conclusions

A series of four Ru(II) sensitizers containing 5 aryl-tetrazolato -based ligands was investigated with the aim of elucidating their structure-related electronic properties and charge transfer dynamics when employed for n-type spectral sensitization. Synthetic routes for ligand structures bearing the 2-pyridyl substituent (**D2**) and with stronger electron withdrawing pyrazine ring (**D1**) were established, followed by the preparation of a further unprecedented class of tetrazolato-based Ru(II) dyes, where decoration of the traditional fragment cis-(bpy-4,4'-dicarboxylate)ruthenium(II) with two 5-aryl tetrazolato (**D3** and **D4**) was carried out, leading to new examples of thiocyanate free dyes. TDDFT calculations have shown that all the new dyes possess excited states with a prevailing MLCT character, with a good directionality for n-type sensitization, while the combination of computation, electrochemical and spectroscopic analysis established ground and excited state thermodynamic properties well suited for efficient interfacial charge separation. This was confirmed by transient absorption spectroscopy in the ns/ms time scale and by internal and external quantum yields of photon to electron conversion ≥ 80% in a Li^+ and Mg^{2+} rich electrolyte. Among the **D** series, the best performance were shown by complexes **D3** and **D4**, owing to the combination of broad harvesting, efficient regeneration by iodide (> 90 %) and nearly unitary quantum yields of electron injection. Compared to the standard N719, the main limitation of this new class of Ru(II) sensitizers arises from their narrower and blue shifted spectral response, originating from the stronger stabilization of the dπ orbitals of Ru(II) induced by the tetrazolato moieties, which limits photoconversion at λ < 700 nm.

View Article Online
DOI: 10.1039/D0DT02621B

EXPERIMENTAL SECTION

General considerations. All the reagents and solvents were obtained commercially (e.g. Alfa-Aesar) and used as received without any further purification, unless otherwise specified. All the reactions were carried out under an argon atmosphere following Schlenk protocols. ESI-mass spectra were recorded using a Waters ZQ-4000 instrument (ESI-MS, acetonitrile as the solvent). Nuclear magnetic resonance spectra (consisting of ^{1}H, and ^{13}C experiments) were always recorded using a Varian Mercury Plus 400 instrument (^{1}H, 400.1) at room temperature. ^{1}H chemical shifts were referenced to residual solvent resonances. Absorption spectra were recorded at room temperature using a Perkin Elmer Lambda 35 UV/vis spectrometer. Uncorrected steady-state emission and excitation spectra were recorded on an Edinburgh FLSP920 spectrometer equipped with a 450 W xenon arc lamp, double excitation and single emission monochromators, and a Peltier-cooled Hamamatsu R928P photomultiplier tube (185−850 nm). Emission and excitation spectra were corrected for source intensity (lamp and grating) and emission spectral response (detector and grating) by a calibration curve supplied with the instrument. The wavelengths for the emission and excitation spectra were determined using the absorption maxima of the MLCT transition bands (emission spectra) and at the maxima of the emission bands (excitation spectra).

Cyclic voltammetry measurements were performed on a Autolab PGSTAT302N potentiostat using a glassy carbon 492/GC/3 (diameter: 4 mm) or a platinum solid 492/PT/2 (diameter: 2 mm) as working electrode and a SCE 303/SCG/6 reference electrode (Amel electochemistry instruments); scan rates 100 $mV{\cdot}s^{-1}$ were applied. The experiments were carried out in degassed CH_3CN/CH_3OH 1:1 (v/v) (spectroscopy grade) solutions containing 0.1 M $[Bu_4N][PF_6]$. The recorded potentials have been referred to the redox couple Fc^{+}/Fc (ferricenium|ferrocene), which displayed $E_{1/2}$ = 0.33 V vs. SCE in the same experimental conditions (at 298 K, from CH_3CN/CH_3OH 1:1 (v/v) solutions containing 0.1 M $[Bu_4N][PF_6]$ as the supporting electrolyte).

Ligand synthesis. Tetrazole derivatives are used as components for explosive mixtures. In this lab, the reactions described here were only run on a few grams scale and no problems were encountered. However, *great caution* should be exercised when handling or heating compounds of this type.

TphCN, **TPYZ** and **PTZ** were obtained by following the general method reported by Finnegan and co-workers.[5]

TphCN (Y = 66%). ^{1}H-NMR: (400 MHz, DMSO-d^6) δ (ppm) = 8.06 (d, 2H, $J_{H\text{-}H}$ = 3.99 Hz), 8.31 (d, 2H, $J_{H\text{-}H}$ = 7.99 Hz);

TPYZ (Y = 64%), ^{1}H-NMR: (400 MHz, DMSO-*d*^{6}) δ (ppm) = 9.37 (d, 1H, J_{H-H} = 4.6 Hz), 8.85 (m, 2H).

PTZ (Y = 62%), ^{1}H-NMR: (400 MHz, DMSO-*d*^{6}) δ (ppm) = 8.76 (d, 2H, J_{H-H} = 3.99 Hz), 8.19 (d, 1H, J_{H-H} = 4.6 Hz) 8.04 (m, 1H), 7.59 (m, 1H).

TphBr was obtained by following the procedure from Koguro and co-workers (Y = 84%).[6] ^{1}H-NMR: (400 MHz, DMSO-*d*^{6}) δ (ppm) = 7.98 (d, 2H, J_{H-H} = 5.99 Hz), 7.81 (d, 2H, J_{H-H} = 5.99 Hz);

General Procedure for the Preparation of the *cis*-[Ru(N^N)$_2$(L)]$^+$[BF$_4$]$^-$-Type Complexes

cis-[Ru(dcbpy)$_2$Cl$_2$] (0.066 g, 0.10 mmol) was dissolved in methanol (60 mL) in a 100 mL round-bottom flask protected from light. A slight excess (2.2 equiv) of $AgBF_4$ was added, and the mixture was stirred at reflux for 3 h. The reaction mixture was filtered through a Celite pad, and the filtrate was added dropwise to a methanol (5 mL) solution of the appropriate tetrazolato ligand (1.6 equiv). Once the addition was complete, the deep-red solution was stirred at reflux temperature overnight. The mixture was then cooled to r.t., concentrated to about half of the initial volume and a copious amount of diethyl ether was added, causing the precipitation of a crude product, which was collected by suction filtration.

D1 ^{1}H-NMR: (CD_3OD, 400 MHz) δ (ppm) = 9.5 (s, 1H), 9.17 (m, 2H), 9.12 (m, 2H), 8.42 (d, 2H), 8.2 (d, 1H), 8.15 (d, 1H), 8.05 (m, 2H), 7.95 (m, 3H), 7.9 (m 1H), 7.43 (m, 1H,). **ESI-MS** (m/z) CH_3CN: $[M]^+$ = 823, $[M]^-$ = 87. Anal. Calcd. For $C_{29}H_{19}N_{10}O_8B_1F_4Ru_1$ (823.41) C 42.3, H 2.33, N 17.01. Found: C 42.5, H 2.36, N 17.03.

D2 ^{1}H-NMR: (CD_3OD, 400 MHz) δ (ppm) = 9.17 (m, 2H), 9.12 (m, 2H), 8.42 (d, 2H), 8.1 (m, 3H), 8.05 (d, 1H), 7.99 (m, 3H), 7.89 (m, 2 H), 7.68 (m 1H), 7.43 (t, 1H). **ESI-MS** (m/z) CH_3CN: $[M^+]$ = 823, $[M^-]$ = 87. Anal. Calcd. For $C_{30}H_{20}N_9O_8B_1F_4Ru_1$ (822.43) C 43.8, H 2.45, N 15.33. Found: C 44.1, H 2.48, N 15.36.

General Procedure for the Preparation of the neutral *cis*-[Ru(N^N)$_2$(L)$_2$]-Type Complexes

cis-[Ru(dcbpy)$_2$Cl$_2$] (0.046 g, 0.07 mmol) was dissolved in methanol (80 mL) in a 250 mL round-bottom flask protected from light. A slight excess (2.2 equiv) of $AgBF_4$ was added, and the mixture was stirred at reflux for 3 h. The reaction mixture was filtered through a celite pad, and the filtrate was added dropwise to a methanol (5 mL) solution of the appropriate tetrazolato ligand (2.2 equiv). Once the addition was complete, the deep-red solution was stirred at reflux temperature overnight. The mixture was then cooled to r.t., concentrated to about half of the initial volume and a copious amount of diethyl ether was added, causing the precipitation of a crude product, which was collected by suction filtration.

View Article Online
DOI: 10.1039/D0DT02621B

D3 ^{1}H-NMR: (CD_3OD, 400 MHz) δ (ppm) = 10.04 (d, 2H, J_{H-H} = 3.9 Hz), 9.02 (s, 2H), 8.90 (s, 2H), 8.18 (m, 2H), 8.02 (m, 2H), 7.97 (d, 4H, J_{H-H} = 7.9 Hz), 7.74 (m, 2H), 7.70 (d, 4H, J_{H-H} = 7.9 Hz). **ESI-MS** (m/z) CH_3CN: $[M+Na]^+$ = 952. Anal. Calcd. For $C_{40}H_{24}N_{14}O_8Ru_1$ (929.8) C 51.67, H 2.60, N 21.09. Found: C 51.75, H 2.68, N 21.1.

D4 ^{1}H-NMR: (CD_3OD, 400 MHz) δ (ppm) = 10.03 (d, 2H, J_{H-H} = 7.9 Hz), 8.98 (s, 2H), 8.85 (s, 2H), 8.12 (m, 2H), 7.78 (m, 2H), 7.70 (d, 4H, J_{H-H} = 7.9 Hz), 7.53 (m, 2H), 7.48 (d, 4H, J_{H-H} = 7.9 Hz). **ESI-MS** (m/z) CH_3CN: $[M+Na]^+$ = 1058. Anal. Calcd. For $C_{38}H_{24}N_{12}O_8Br_2Ru_1$ (1037.57) C 43.99, H 2.33, N 16.2. Found: C 44.05, H 2.39, N 16.4.

DSSC assembly and characterization. The TiO_2 inks were deposited onto Fluorine-doped Tin Oxide (FTO) glass substrates (sheet resistance 7 Ω/sq, Sigma-Aldrich) using a semi-automatic screen-printer AUR'EL 900, AUR'EL Automation s.p.a., Italy), and treated at 450°C for 30 minutes.[27] Before this deposition, the substrates were coated with TiO_2 blocking layer (BL), deposited according to a previously reported procedure.[28] Briefly, an ethanolic solution of $TiCl_4$ (50 mM) was spin coated onto the FTO substrates to obtain a thin compact TiO_2 film, and then treated at 450°C for 30 minutes. The thickness of the TiO_2 film (photoanode) was adjusted at about 8 µm. After sintering, the films were immersed in a 50mM $TiCl_4$ aqueous solution at 70°C, and then fired at 450°C for 30 minutes. The as obtained photoanodes were then dipped for 16 hours in as 0.3 mM absolute ethanol solution of each different dyes. As a reference, also DSSCs sensitized with di-Tetrabutylammonium *cis*-bis (isothiocyanato)bis(2,2'-bipyridyl-4,4'-dicarboxylato)ruthenium(II), named N719 dye (Sigma-Aldrich) were prepared. A pre-drilled FTO coated glass covered with a sputtered platinum layer was used as the counter electrode. After the photoanode sensitization the electrodes were assembled into a sandwich type cell and sealed with a hot melt gasket made of Meltonix (thickness 25 µm, Solaronix, Switzerland). Different Electrolytes were used, consisting in either a custom formulated electrolyte (CFE) comprised of 0.1 M LiI (99.999 % Sigma Aldrich), 0.6 M 1-Methyl-3-Propylimidazolium iodide (PMII) (ACS grade ≥ 98%, Sigma Aldrich), 0.05 M MgI_2 (> 99% (Fluka)) and 0.1 M I_2 (> 99.8 %, Sigma Aldrich) in CH_3CN (> 99.8 %, Sigma Aldrich) or with a commercial optimized electrolyte for NCS containing dyes (Iodolyte Z100, Solaronix, Switzerland). The electrolyte was introduced in the cell via vacuum back filling through the hole in the counter electrode. The active area of the solar cells was fixed at 0.25 cm^2. In order to evaluate the DSSCs performance, current-voltage curves, Electrochemical Impedance Spectroscopy (EIS) and Incident Photon-to-electron-Conversion Efficiency (IPCE) analyses were done. The J-V tests of devices were conducted on a Keithley Model 2400 with an AM 1.5G solar simulator (SUN 2000, Abet

Technologies). The system was calibrated against a certified silicon solar cell and the light intensity of 1000 W m^{-2}. IPCE is determined using PVE300 (Bentham Instrument Ltd, Reading, Berkshire, UK) with dual xenon/quartz halogen light source, measured in DC mode and no bias light is used. Electrochemical Impedance Spectroscopy measurements were recorded using AutoLab PGSTAT302N+FRA32 (Metrohm Autolab, The Nederlands) in the dark at open circuit voltage. An alternating sinusoidal signal of 10 mV and frequency range from 100 KHz to 0.1 Hz were used. The experimental points of impedance spectra were fitted with Z-View software (Scribner Associates Inc.).

Transient Absorption Spectroscopy. Transient Absorption Spectroscopy in the ns-ms time scale was carried out with a previously described time resolved spectrometer.[29] Briefly, the samples either consisting of sensitized TiO_2 thin films or methanolic dye solutions were excited by the 532 nm harmonic of a nanosecond Nd:YAG laser (Continuum Surelite II) attenuated to *ca.* 3.3 mJ/pulse/cm^2 by using a defocusing lens and neutral filters. Sensitized TiO_2 thin films in contact with the selected electrolytes (CFE, Z100 Iodolyte, 0.1 M $LiClO_4$ (≥99 %, Acros) in CH_3CN) were kept in quartz cell and oriented at an angle of *ca.* 45° with respect to the laser beam, in order to reflect scattered laser light away from the detector (R3896 photomultiplier attached to an Acton triple grating monochromator where the 50 lines/mm grating was selected). A stack of two 532 nm notch filters placed at the entrance of the detector further eliminated residual 532 nm radiation scattered by the sample. The white light probe beam generated by a 150 W Xe lamp was orthogonal with respect to the laser source. Pulsing of the Xe lamp was optional, and could be exploited within a time window lower than 400 μs in order to improve the S/N ratio of the transient signals. The probe light was filtered through a 380 nm cut off filter in order to remove most of high frequency UV radiation before being focused into the sample by means of a cylindrical lens and being collected. Depending on the time frame to be explored, in order to optimize the S/N ratio of the oscillographic traces, various oscilloscope impedances were used, ranging from 50 Ω to 10 kΩ. Usually from 10 to 30 laser shots at a frequency of 0.2 Hz at each sampled wavelength were averaged. Each trace (ΔA vs time) was fitted with a multiexponential decay function in order to further reduce stochastic noise and fluctuations and the resulting fitting function was used to build time resolved spectra.

Quantum Chemical Computations. Geometry optimization of the dye structures was performed with Gaussian 09 A2 [30] at the restricted DFT-pbe0/DGDZVP level *in vacuo* with tight convergence criteria. TDDFT spectra (lowest 25 singlet transitions) were computed in CH_3OH according to the polarizable dielectric continuum model (IEFCPM). Kohn Sham (KS) molecular orbitals were visualized

View Article Online
DOI: 10.1039/D0DT02621B

as isodensity surfaces with Gaussview 5. Wavefunction analysis and EDDM (Electron Density Difference MAPS) of the optical transitions were obtained with Multiwfn 3.3.9.[31] The oxidation potential of the lowest singlet excited state, whose $^{S}E^{00}$ spectroscopic energy is not experimentally accessible from steady state emission spectroscopy, was calculated from the lowest computed vertical excitation energy according to $^{S}E_{ox}^{*} = E_{ox} - {}^{S}E^{00}$. The triplet excited state potential was calculated in a similar fashion by using the spectroscopic energy $^{T}E^{00}$ from the onset of the emission spectrum according to the 10% intensity criterion (Figure S8).[32]

Conflicts of Interests. There are no conflicts to declare.

Acknowledgments The authors wish to thank the Toso Montanari Foundation for financial support. E. M. thanks the Fondo Sociale europeo Programma Operativo (2014–2020) Regione Emilia Romagna for a grant.

References

[1] a) M. Dinca, A. Dailly, Y. Liu, C. M. Brown, D. A. Neumann, and J. R. Long H., *J. Am. Chem. Soc.* **2006**, *128*, 16876-16883; b) Zhao, Z.-R. Qu, H.-Y. Ye, and R.-G. Xiong, *Chem. Soc. Rev.* **2008**, *37*, 84-100 and references cited therein.

[2] G. Steinhauser and T. M. Klapötke, *Angew. Chem. Int. Ed.* **2008**, *47*, 3330 –3347.

[3] a) N. M. Shavaleev, S. V. Eliseeva, R. Scopelliti and J.-C. G. Bünzli, *Inorg. Chem.* **2014**, *53*, 5171−5178; b) D. D'Alessio, S. Muzzioli, B. W. Skelton, S. Stagni, M. Massi and M. I. Ogden, *Dalton Trans.,* **2012**, *41*, 4736–4739.

[4] a) C. Dragonetti, A. Colombo, M. Magni, P. Mussini, F. Nisic, D. Roberto, R. Ugo, A. Valore, A. Valsecchi, P. Salvatori, M. G. Lobello and F. De Angelis, *Inorg. Chem.*, **2013**, *52*, 10723-10725; b) A. Colombo, C. Dragonetti, M. Magni, D. Meroni, R. Ugo, G. Marotta, M. G. Lobello, P. Salvatori and F. De Angelis, *Dalton Trans.*, **2015**, *44*, 11788; c) G. Wu, R. Kaneko, Y. Zhang, Y. Shinozaki, K. Sugawa, A. Islam, L. Han, I. Bedja, R. K. Gupta, Q. Shen and J. Otsuki, *J. Power Sources*, **2016**, *307*, 416-425.

[5] W. G. Finnegan, R. A. Henry and R. Lofquist; *J. Am. Chem. Soc.* **1958**, *80*, 3908-3911.

[6] K. Koguro, T. Oga, S. Mitsui and R. Orita; *Synthesis* **1998**, 910–914.

[7] S. Trasatti, *Pure Appl. Chem*., **1986**, *58*, 955-966.

[8] S. Stagni, E. Orselli, A. Palazzi, L. De Cola, S. Zacchini, C. Femoni, M. Marcaccio, F. Paolucci, and S. Zanarini, *Inorg. Chem.*, **2007**, *46*, 9126-9138.

[9] M.K. Nazeeruddin, S. M. Zakeeruddin, R. Humphry-Baker, M. Jirousek, P. Liska, N. Vlachopoulos, V. Shklover Christian-H. Fischer, M. Gratzel; *Inorg. Chem.*, **1999**, *38*, 6298-6305.

[10] M. K. Nazeeruddin, A. Kay, I. Rodicio, R. Humphry-Baker, E. Müller, P. Liska, N. Vlachopoulos and M. Grätzel, *J. Am. Chem. Soc*., **1993**, *115*, 6382-6390.

[11] L. A. Fredin and T. C. Allison, *J. Phys. Chem. A*, **2016**, *120*, 13, 2135-2143.

[12] a) M. Pastore, A. Selloni, S. Fantacci and F. De Angelis; In *"Electronic and Optical Properties of Dye-Sensitized TiO_2 Interfaces"*; Springer: Berlin, **2014**, 1−45; b) G. Prampolini, F. Ingrosso, A. Segalina, S. Caramori, P. Foggi and M. Pastore, *J. Chem. Theory Comput.,* **2019**, *15*, 529−545.

[13] M. Cossi, V. Barone, R. Cammi and J. Tomasi, *Chem. Phys. Lett*., **1996**, *255*, 327−335.

[14] G. Wolfbauer, A. M. Bond, G. B. Deacon, D. R. MacFarlane and L. Spiccia, *J. Am. Chem. Soc*., **2000**, *122*, 130-142.

[15] S. Fantacci and F. De Angelis*, Coord. Chem. Rev.*, **2011**, *255*, 2704−2726.

View Article Online
DOI: 10.1039/D0DT02621B

[16] a) R. Englman and J. Jortner; *Molecular Physics,* **1970**, *18*, 145-164; b) J.V. Caspar and T.J. Meyer; *J. Phys. Chem.*, **1983**, *87*, 952-957.

[17] M. Borgwardt, M. Wilke, T. Kampen, S. Mähl, W. Xiang, L. Spiccia, K. M. Lange, I. Y. Kiyan and E. F. Aziz, *J. Phys .Chem C*, **2015**, *119*, 9099, 9107.

[18] S. E. Koops, B. C. O'Regan, P. R. F. Barnes and J. R. Durrant, *J. Am. Chem. Soc.*, **2009**, *131*, 4808.

[19] S. K. Balasingam, M. Lee, M. G. Kang and Y. Jun, *Chem. Commun.*, **2013**, *49*, 1471. The flat band potential of TiO_2 is strongly dependent on the details of formulation of the electrolyte medium, see for example G. Redmond and D. Fitzmaurice, *J. Phys. Chem*. *B*, **1993**, *97*, 1426.

[20] J. R. Durrant, S. A. Haque and E. Palomares, *Coord. Chem. Rev*., **2004**, *248*, 1247-1257.

[21] G. Boschloo, E. A. Gibson and A. Hagfeldt, *J. Phys. Chem. Lett*., **2011**, *2*, 3016-3020.

[22] W. Song, M. K. Brennaman, J. J. Concepcion and J. W. Jurss; *J. Phys. Chem. C*, **2011**, *115*, 7081−7091.

[23] M. Ambily, A. Venu, G. Mohan Rao and N. Munichandraiah, *Electrochim. Acta,* **2013**, *87*, 92-96.

[24] a) A. Agresti, S. Pescetelli, E. Gatto, M. Venanzi and A. Di Carlo, *J. Power Sources*, **2015**, *287*, 87-95; b) A. Agresti, S. Pescetelli, A. Quatela, S. Mastroianni, T. M. Brown, A. Reale, C. A. Bignozzi, S. Caramori, A. Di Carlo; *RSC Adv*., **2014**, *4*, 12366-12375; c) D. Perganti, A. G.Kontos, T. Stergiopoulosa, V. Likodimos, J. Farnell, D. Milliken, H. Desilvestro, P. Falaras; *Electrochim. Acta*, **2015**, *179*, 241-249.

[25] a) E. Benazzi, M. Magni, A. Colombo, C. Dragonetti, S. Caramori, C.A.. Bignozzi, R. Grisorio, G.P. Suranna, M.P. Cipolla, M. Manca, and D. Roberto, *Electrochim. Acta* **2018**, *271*, 180.

[26] S. Sarker, A.J.S. Ahammad, H.W. Seo, and D.M. Kim, *Int. J. Photoenergy,* **2014,** *2014*, Article ID 851705.

[27] R. Bendoni, N. Sangiorgi, A. Sangiorgi and A. Sanson; *Solar Energy*, **2015**, *122*, 497-507.

[28] A. Sangiorgi, R. Bendoni, N. Sangiorgi, A. Sanson and B. Ballarin; *Ceramics International*, **2014,** 40, 10727-10735.

[29] F. Ronconi, M -P. Santoni, F. Nastasi, G. Bruno, R. Argazzi, S. Berardi, S. Caramori, C. A. Bignozzi and S. Campagna, *Dalton Trans.,* **2016**, *45*, 14109.

[30] M. J. Frisch, G. W. Trucks, H. B. Schlegel, G. E. Scuseria, M. A. Robb, J. R. Cheeseman, G. Scalmani, V. Barone, B. Mennucci, G. A. Petersson, H. Nakatsuji, M. Caricato, X. Li, H. P. Hratchian, A. F. Izmaylov, J. Bloino, G. Zheng, J. L. Sonnenberg, M. Hada, M. Ehara, K. Toyota, R. Fukuda, J. Hasegawa, M. Ishida, T. Nakajima, Y. Honda, O. Kitao, H. Nakai, T. Vreven, J. A. Montgomery Jr., J. E. Peralta, F. Ogliaro, M. J. Bearpark, J. Heyd, E. N. Brothers, K. N. Kudin, V. N. Staroverov, R. Kobayashi,

View Article Online
DOI: 10.1039/D0DT02621B

J. Normand, K. Raghavachari, A. P. Rendell, J. C. Burant, S. S. Iyengar, J. Tomasi, M. Cossi, N. Rega, N. J. Millam, M. Klene, J. E. Knox, J. B. Cross, V. Bakken, C. Adamo, J. Jaramillo, R. Gomperts, R. E. Stratmann, O. Yazyev, A. J. Austin, R. Cammi, C. Pomelli, J. W. Ochterski, R. L. Martin, K. Morokuma, V. G. Zakrzewski, G. A. Voth, P. Salvador, J. J. Dannenberg, S. Dapprich, A. D. Daniels, Ö. Farkas, J. B. Foresman, J. V. Ortiz, J. Cioslowski, D. J. Fox; Gaussian 09 Revison A.02.

[31] L. Tian and C. Feiwu, *J. Comput. Chem*., **2012**, *33*, 580–592.

[32] A. Døssing, C. K. Ryu, S. Kudo and P.C. Ford, *J. Am. Chem. Soc.* **1993**, *115*, 5132–5137.

New examples of Ru(II)-tetrazolato complexes as thiocyanate-free sensitizers for Dye-Sensitized Solar Cells

View Article Online
DOI: 10.1039/D0DT02621B

Valentina Fiorini,[a] Edoardo Marchini,[b] Mattia Averardi,[a] Loris Giorgini,[a] Sara Muzzioli,[a] Angela Dellai,[b] Roberto Argazzi,[b] Alessandra Sanson,[c] Nicola Sangiorgi,[c]* Stefano Caramori,[b]* Stefano Stagni [a]*

Graphical Abstract

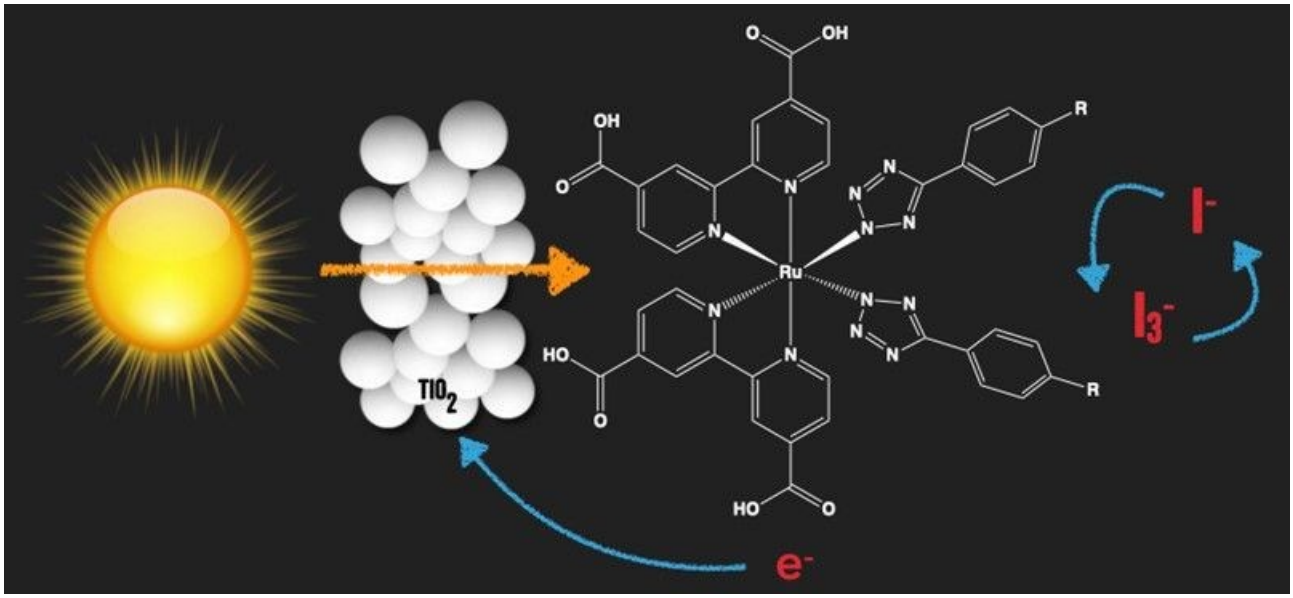

Text: Newly designed Ru(II) tetrazolato complexes as thiocyanate-free dyes for Ru-based DSSCs.